ISOLATION OF RESONANT WAVE FEATURES IN LOW-FREQUENCY WIDEBAND SAS DATA PRODUCTS FROM CYLINDRICAL SHELLS

AJ Hunter University of Bath
Z Rymansaib Bath, BA2 7AY, United Kingdom
CJ Sanford

BW Thomas Atlas Elektronik UK
A Burt Dorchester, DT2 8ZB, United Kingdom
R Brothers

1 INTRODUCTION

Low-frequency wideband synthetic aperture sonar (SAS) data products can contain features corresponding to acoustic and elastic wave interactions with objects of interest. These features can convey potentially useful information on an object's internal structure and composition for automated recognition. However, they are more difficult to interpret than conventional geometric features from high-resolution, high-frequency SAS images due to the more complicated wave physics. This paper explores the isolation of such features caused by resonant elastic waves. We explore Lamb, Scholte, and other wave resonances in a variety of cylindrical shells and show how these features can be isolated across multiple data products, including frequency-aspect plots and complex images. Simulated and experimental results are presented at frequencies up to 100 kHz for three different aluminium shells: a 600x300x12.5 mm (length x outer diameter x thickness) cylinder in the free field, and 500x200x5 mm and 850x170x5 mm cylinders both in the free field and on the seabed.

2 ELASTIC WAVE MODES

We expect to observe resonant features in the backscattered echoes relating to various elastic wave phenomena that can exist in cylindrical shells [1]. These can be supported by the whole body as flexural, longitudinal, and torsional waves, and within the shell wall as Lamb waves. Furthermore, the inner and outer surfaces can support quasi-Scholte waves at the interfaces between the external water and internal filling. Figure 1 shows the wave speeds of various modes in water-loaded aluminium cylindrical shells of thickness 12.5 mm and 5 mm, approximated locally as infinite flat plates; these were produced using the Disperse software [2].

2.1 Lamb Waves

Lamb waves are propagating elastic waves that oscillate in a direction out of the wall's plane and are guided by its boundaries. They can exist in various orders of symmetric and asymmetric modes, termed S0, S1, S2, … and A0, A1, A2, …, respectively for the zeroth, first, and second order, etc. Lamb waves can be established by coupling into the wall from acoustic pressure waves in the water. Approximating the wall locally as an infinite flat plate, this happens at angles

$$\Phi(f) = \cos^{-1}(c_W / c(f)) \quad (1)$$

relative to the surface normal and is dependent on the frequency f, the constant wave speed in water $c_W \approx 1{,}500\ \mathrm{m/s}$, and the dispersive speed $c(f)$ for the particular Lamb wave (c.f. Figure **1**).

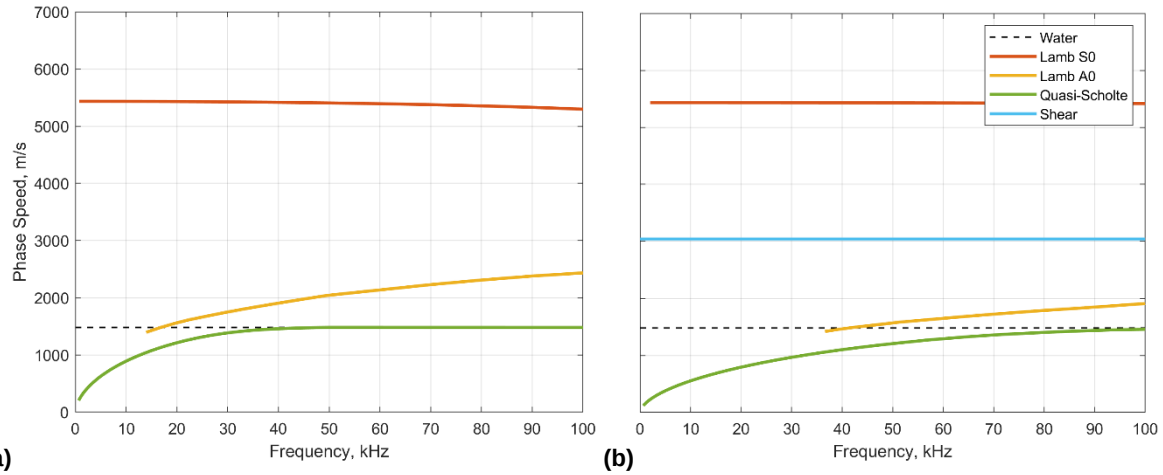

Figure 1 *– Dispersion curves for infinite flat water-loaded aluminium plates of thicknesses (a) 12.5 mm and (b) 5 mm.*

Note that the coupling angles become complex at frequencies where the Lamb wave speed is below the water speed and, therefore, coupling with acoustic waves in the fluid is not possible under this condition.

Consider an incident planar pressure wave travelling in the plane containing the cylinder's axis at an angle α relative to the "broadside" angle. Coupling can occur when the wavelengths in the water and wall match. This happens at a circumferential angle

$$\beta(f) = \cos^{-1}(- \mathrm{c_W} \,/\, (\mathrm{c(f)}\cos(\alpha))), \tag{2}$$

leading to a Lamb wave propagating at a helical angle

$$\gamma(f) = \cos^{-1}\big(\sin(\alpha) \,/\, \sin\big(\Phi(f)\big) \big) \tag{3}$$

relative to the cylinder's axis [3] [4]. Thus, a complete continuum of helical waves will be established between the meridian ($\beta = 0, \gamma = 0$) and the circumference ($\gamma = 90\,\mathrm{deg}$, $\beta = \Phi$) for incident angles between $\alpha = \Phi$ and $\alpha = 0$, respectively. Note that the coupling angles become complex for $\alpha > \Phi$ and coupling is therefore not possible under this condition.

Constructive reinforcement of the Lamb waves occurs when the circumferential path is an integer multiple $n \in \mathbb{Z}$ of wavelengths, leading to the resonance condition

$$\alpha_n(f) = sin^{-1}\left(\frac{c_W}{c(f)}\sqrt{1 - \left(\frac{n}{2\pi R}\cdot\frac{c(f)}{f}\right)^2}\right), \tag{4}$$

where R is the radius of the cylinder.

2.2 Quasi-Scholte Waves

Scholte waves are evanescent waves that can exist on the boundary of a fluid and solid half space. They are non-dispersive and travel along the boundary at a speed that is slightly below the wave speed in the fluid. Quasi-Scholte waves can exist on each of the two boundaries of a plate and approach two independent Scholte waves asymptotically in the high-frequency limit. They are dispersive below this limit.

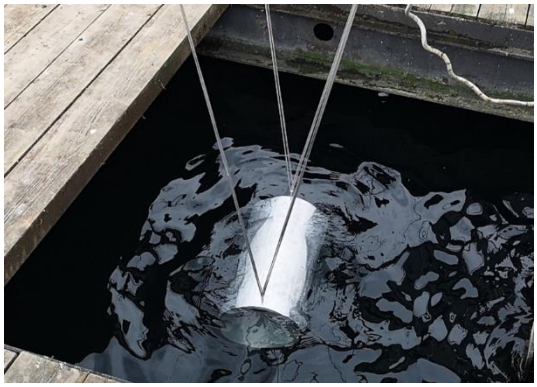

Figure 2 *– Suspension of the 600x300x12.5 mm cylindrical aluminium shell for measurement at Wraysbury Reservoir. The shell was suspended mid-water at 8 m depth.*

The quasi-Scholte wave speed never exceeds the fluid speed (c.f. Figure **1**). Therefore, coupling from the water into subsonic quasi-Scholte waves should not be possible in the same way that it is for supersonic Lamb waves. In any case, Scholte waves that have been established in a cylindrical shell will follow helical paths and create resonances in the same manner as Lamb waves and can also be described by equation (4) but using the quasi-Scholte wave speed $c(f)$ instead.

3 EXPERIMENTS AND SIMULATIONS

Experimental measurements and finite-element simulations have been conducted on various cylindrical shells by both the University of Bath (in collaboration with the National Physical Laboratory and DSTL) and Atlas Elektronik UK (AEUK). We present a selection of results from three aluminium cylindrical shells with different geometries. Moreover, we attempt to use knowledge of the elastic wave physics to isolate and understand observable features in these data.

3.1 12.5 mm Wall Thickness (University of Bath)

A 600x300x12.5 mm (length x outer diameter x thickness) cylindrical aluminum shell has been measured experimentally in the free-field at Wraysbury Reservoir (see Figure 2) and simulated numerically using an axi-symmetric finite-element model in COMSOL. The experimental measurements were made using wideband chirp signals over two bands covering up to 100 kHz. The object was rotated continuously over 720 deg, yielding measurements at angular increments of 0.25 deg. The simulations covered frequencies up to 30 kHz in 100 Hz increments and angles from 0 to 90 deg (expanding to a complete 360 deg under symmetry) in angular increments of 0.5 deg.

The frequency-aspect acoustic colour representation of the experimentally measured data is shown in Figure 3. The predicted resonances of the A0 and S0 Lamb waves and the quasi-Scholte waves of equation (4) have been overlaid. The predicted onset of the A0 modes can be observed above approximately 15 kHz. Moreover, the superposition of the meridional A0 modes can be observed at the wider angles. This can also be observed for the meridional S0 modes, and both are most apparent at the higher frequencies above approximately 30 kHz.

The presence of features aligning with the predicted quasi-Scholte wave resonances was unexpected. There is a convincing correspondence in both the experimental results of Figure 3 and the simulated results of Figure 4, but at alternating modes rather than each one. We hypothesize that these resonances have been initiated and re-radiated via scattering at the cylinder's terminations. We have used SAS imaging to explore this hypothesis.

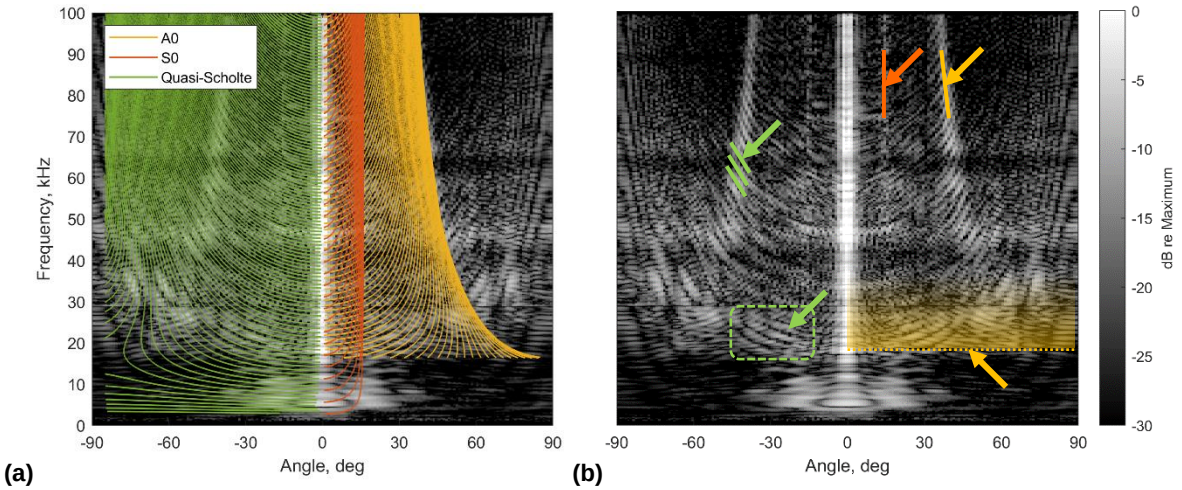

Figure 3 *– Frequency-aspect acoustic colour representation of experimental measurements from the 600x300x12.5 mm cylindrical shell. Theoretical Lamb and Scholte resonances are overlaid in (a) and their observable features are indicated in (b), highlighting superposition of the A0 and S0 resonant modes, onset of the A0 modes at ~15 kHz, and possible presence of Scholte resonant modes.*

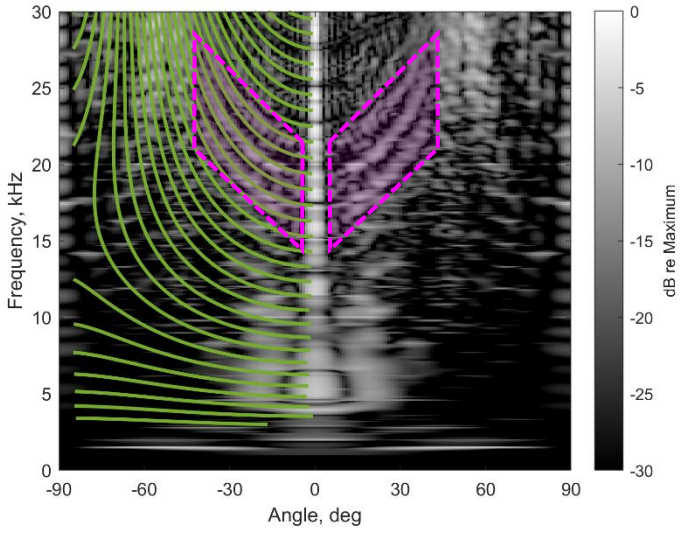

Figure 4 *– Frequency-aspect acoustic colour representation of simulated measurements from the 600x300x12.5 mm cylindrical shell. The possible Scholte wave resonances have been annotated in green. Three corresponding features were isolated using the windows indicated in magenta for subsequent SAS imaging.*

Semi-circular SAS images of the cylinder were produced over 0-30 kHz for angles between -45 and +45 deg relative to broadside. These images are shown in Figure 5(a) and Figure **5**(c) for the experiments and simulations, respectively. There is a prominent geometric reflection from the broadside surface as well as a significant “tail” caused by the elastic resonances. Three features corresponding to the possible quasi-Scholte waves were isolated by windowing them in the frequency-aspect representation, as shown in Figure 4. The SAS images produced from these windowed data products are shown in Figure 5(b) and Figure **5**(d). They show that the features are localised near the cylinder’s ends, thus supporting the hypothesis of scattering as the mechanism for initiation and re-radiation of Scholte waves.

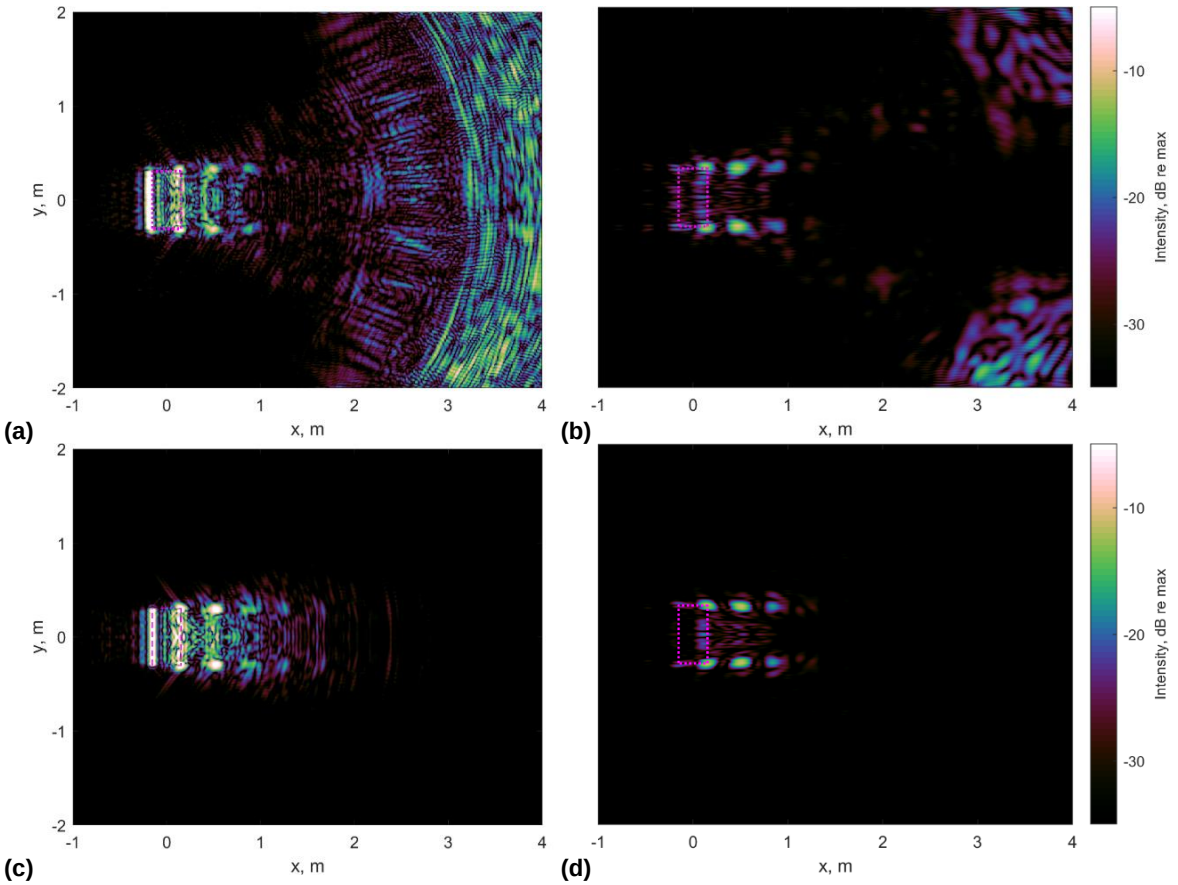

Figure 5 *– Circular SAS images over 0-30 kHz and ±45 deg relative to broadside for (top row; a, b) experimental measurements of the 600x300x12.5 mm cylindrical shell and (bottom row; c, d) simulations of the same shell. Full SAS images are on the left (a,c) and images of the isolated quasi-Scholte modes are on the right (b,d). The geometric outlines of the objects are indicated in magenta.*

3.2 5 mm Wall Thickness (Atlas Elektronik UK)

Two cylindrical aluminium shells of dimensions 500x200x5 mm and 850x170x5 mm have been simulated numerically in the free-field using COMSOL and measured experimentally on the seafloor using AEUK's low-frequency SAS system, operating over a bandwidth from 8 kHz to 32 kHz. These shells are thinner than the one presented in the previous section. Therefore, they do not support as many resonant Lamb wave modes in the shell wall over the frequencies of interest.

The frequency-aspect acoustic colour representations produced from the simulations are shown in Figure 6. Neither Lamb nor quasi-Scholte wave resonances are obvious. However, some interesting features can be observed for the 850x170 mm cylinder in Figure 6(b). The phase speed of the waves creating these features is close to that of the shear wave speed, and the corresponding resonance predictions have been overlaid for comparison. However, shear waves cannot couple into or re-radiate from the shell wall as they have no out-of-plane displacement. Therefore, we suspect that these features are the result of a flexural wave, whose phase speed trends to the shear wave speed with frequency [5].

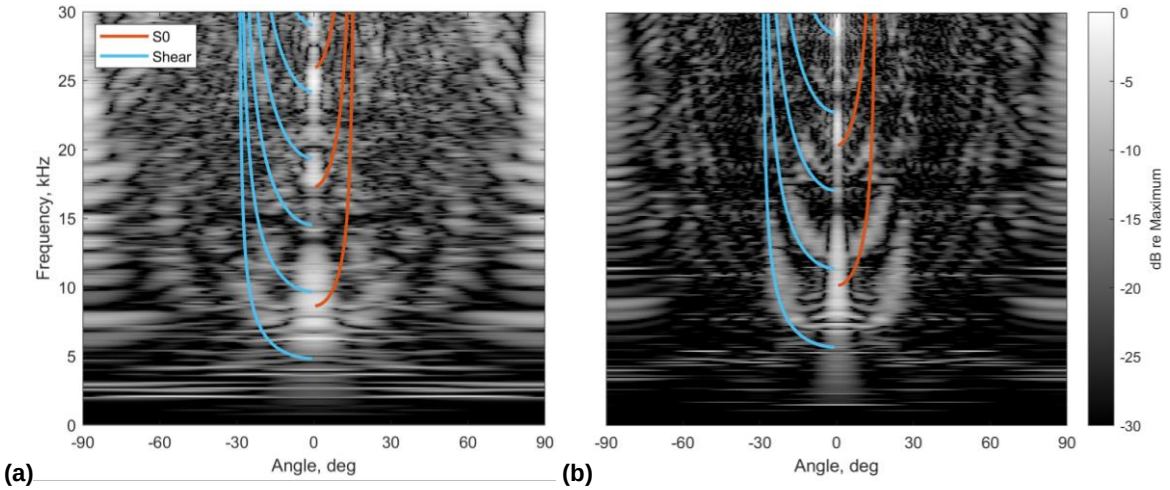

Figure 6 – Frequency-aspect acoustic colour representation of simulated measurements from (a) 500x200x5 mm and (b) 850x170x5 mm cylindrical shells.

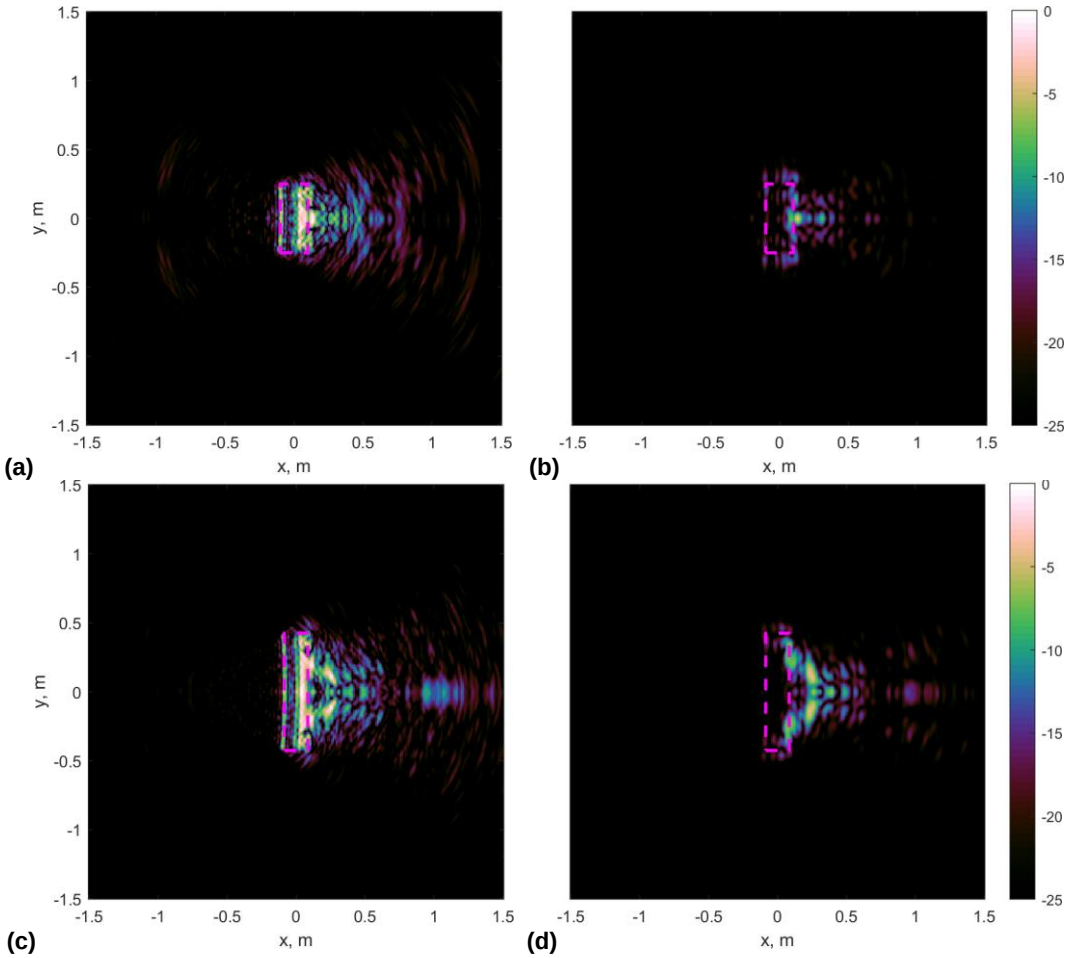

Figure 7 *– Circular SAS images over 0-30 kHz and ±45 deg relative to broadside for simulated measurements of (top row; a, b) 500x200x5 mm cylindrical shell and (bottom row; c, d) 850x170x5 mm shell. Full SAS images are on the left (a,c) and images of the isolated flexural modes are on the right (b,d).*

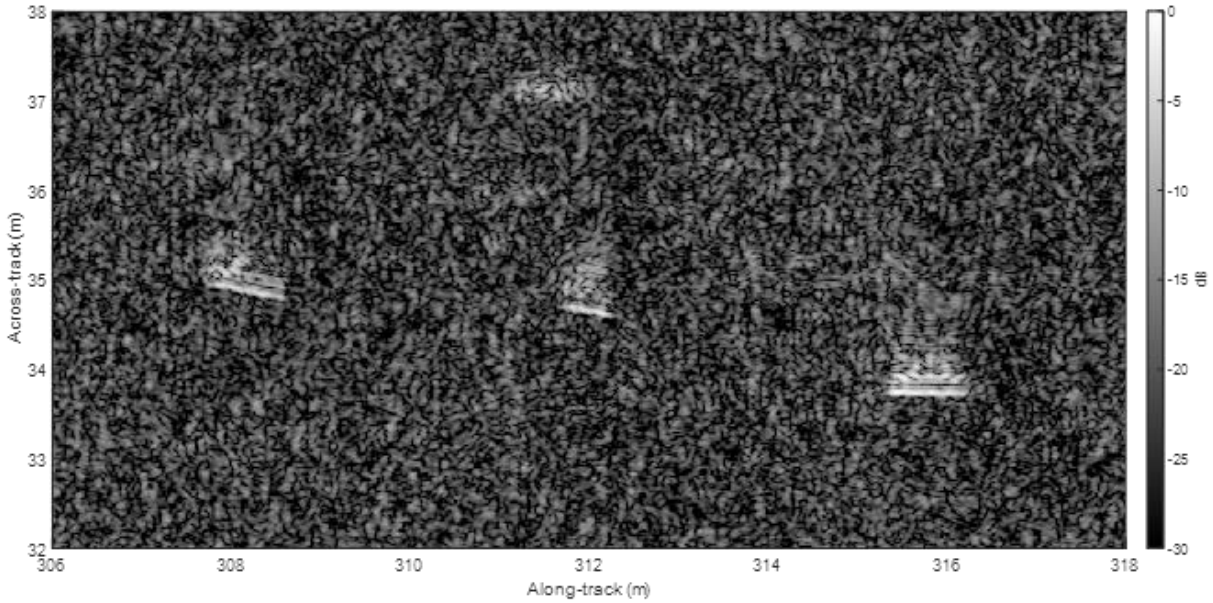

Figure 8 *– SAS image from experimental measurements at 8-32 kHz of a 500x200x5 mm aluminium cylindrical shell flanked by two 850x170x5 mm cylindrical shells on the seafloor.*

The possible flexural wave features were isolated by windowing the frequency-aspect representation followed by semi-circular SAS imaging, as described the previous section. The SAS images are shown in Figure 7. The images show that the isolated features are time delayed and distributed along the lengths of the cylinders. Furthermore, they do not radiate from the cylinder ends, as they do for the quasi-Scholte waves on the thicker cylinder. We therefore postulate that the flexural waves are excited in the cylinder wall, propagate along a helical path, reflect off the cylinder ends, and reradiate from the wall. The exact nature of these flexural waves will be investigated in future research.

Finally, three thin cylindrical shells (two 850x170 mm and one 500x200 mm) have been imaged resting proud on the seabed by a low-frequency SAS operating between 8 kHz and 32 kHz. A SAS image generated from a linear strip-map imaging geometry is shown in Figure 8. The resonant tails can be seen for each of the cylinders. These are observable above the seabed reverberation and exhibit different characteristics for the different objects and aspect angles.

4 CONCLUSIONS

The interpretation of data products from low-frequency wideband SAS systems is complicated due to the elastic wave physics. In this ongoing work, knowledge of elastic wave resonance phenomena is being used to identify and isolate data features that could be useful for enhancing automatic target recognition. It has been shown how features can be isolated in the frequency-aspect acoustic colour representation so that they can be localised in the SAS image.

Data and image features have been observed which are consistent with Lamb waves within the wall of an aluminium cylindrical shell and quasi-Scholte waves on the inner and outer surfaces. The former can directly couple between the water and the wall, whereas there is strong evidence to suggest that the latter are initiated and reradiated via a scattering mechanism at the ends. Other features have been observed, which we speculate are caused by flexural resonance of the entire shell rather than the walls. However, this requires further investigation.

The resonant tails caused by elastic resonances have been observed in experimental measurements from objects resting proud on the seabed. Future work will investigate the detectability and reliability of these features against the background seabed reverberation.

ACKNOWLEDGEMENTS

This work was funded by the UK Defence Science and Technology Laboratory (DSTL) and the Defence and Security Accelerator (DASA). The authors are grateful to Prof. Michael Lowe at Imperial College and Prof. Kevin Williams at University of Washington for helpful discussions on elastic wave modes.

REFERENCES

[1] J. L. Rose, Ultrasonic Guided Waves in Solid Media, Cambridge University Press, 2014.

[2] B. Pavlakovic, M. Lowe, D. Alleyne and P. Cawley, “Disperse: a general purpose program for creating dispersion curves,” in *Review of Progress in Quantitative Nondestructive Evaluation*, 1997.

[3] G. Kaduchak, C. Wassmuth and C. Loeffler, “Elastic wave contributions in high-resolution acoustic images of fluid-filled, finite cylindrical shells in water,” *J. Acoust. Soc. Am.,* vol. 100, no. 64, 1996.

[4] A. Tesei, J. Fawcett and R. Lim, “Physics-based detection of man-made elastic objects buriedin high-density clutter areas of saturated sediments,” *Applied Acoustics,* vol. 69, no. 5, 2008.

[5] D. Alleyne, M. Lowe and P. Cawley, “The reflection of guided waves from circumferential notches in pipes,” *Journal of Applied Mechanics,* vol. 65, pp. 635-641, 1998.